processes

MDPI

Article

Research on Drillability Prediction of Shale Horizontal Wells Based on Nonlinear Regression and Intelligent Optimization Algorithm

Yanbin Zang [1], Qiang Wang [2,*], Wei Wang [3], Hongning Zhang [1], Kanhua Su [2], Heng Wang [1], Mingzhong Li [4], Wenyu Song [4] and Meng Li [2]

[1] SINOPEC Research Institute of Petroleum Engineering Co., Ltd., Beijing 102206, China
[2] Department of Petroleum and Natural Gas Engineering, Chongqing University of Science and Technology, Chongqing 401331, China; 2009038@cqust.edu.cn (K.S.); 2016019@cqust.edu.cn (M.L.)
[3] Sinopec North China Oil & Gas Company, Zhengzhou 450006, China; wangweicq@163.com
[4] Sinopec Huabei Oilfield Service Company, Zhengzhou 450006, China
* Correspondence: wangqiangjjsc@126.com; Tel.: +86-13540622433

Abstract

Shale oil and gas reservoirs are characterized by low porosity and low permeability. The development of ultra-long horizontal wells can significantly increase reservoir contact area and enhance single-well production. Shale formations exhibit distinct bedding structures, high formation pressure, high rock hardness, and strong anisotropy. These characteristics result in poor drillability, slow drilling rates, and high costs when drilling horizontally, severely restricting efficient development. Therefore, accurately predicting the drillability of shale gas wells has become a major challenge. Currently, most scholars rely on a single parameter to predict drillability, which overlooks the coupled effects of multiple factors and reduces prediction accuracy. To address this issue, this study employs drillability experiments, mineral composition analysis, positional analysis, and acoustic transit-time tests to evaluate the effects of mineral composition, acoustic transit time, bottom-hole confining pressure, and formation drilling angle on the drillability of horizontal well reservoirs, innovatively integrating multiple parameters to construct a nonlinear model and introducing three intelligent optimization algorithms (PSO, AOA-GA, and EBPSO) for the first time to improve prediction accuracy, thus breaking through the limitations of traditional single-parameter prediction. Based on these findings, a nonlinear regression prediction model integrating multiple parameters is developed and validated using field data. To further enhance prediction accuracy, the model is optimized using three intelligent optimization algorithms: PSO, AOA-GA, and EBPSO. The results indicate that the EBPSO algorithm performs the best, followed by AOA-GA, while the PSO algorithm shows the lowest performance. Furthermore, the model is applied to predict the drillability of Well D4, and the results exhibit a high degree of agreement with actual measurements, confirming the model's effectiveness. The findings support optimization of drilling parameters and bit selection in shale oil and gas reservoirs, thereby improving drilling efficiency and mechanical penetration rates.

Keywords: long horizontal well; shale oil and gas; intelligent optimization algorithm; drillability prediction

check for updates

Academic Editor: Mohd Azlan Hussain

Received: 20 August 2025
Revised: 9 September 2025
Accepted: 18 September 2025
Published: 22 September 2025

Citation: Zang, Y.; Wang, Q.; Wang, W.; Zhang, H.; Su, K.; Wang, H.; Li, M.; Song, W.; Li, M. Research on Drillability Prediction of Shale Horizontal Wells Based on Nonlinear Regression and Intelligent Optimization Algorithm. *Processes* **2025**, *13*, 3021. https://doi.org/10.3390/pr13093021

Copyright: © 2025 by the authors. Licensee MDPI, Basel, Switzerland. This article is an open access article distributed under the terms and conditions of the Creative Commons Attribution (CC BY) license (https://creativecommons.org/licenses/by/4.0/).

1. Introduction

In recent years, shale oil and gas reservoirs have become a focal point of exploration and development and are regarded as a key growth area for hydrocarbon resources. However, due to the deep burial of shale formations (typically below 3000 m), distinct bedding structures, high formation pressure, high rock hardness, and strong anisotropy, drilling rates remain slow and costs high, significantly constraining efficient development. Therefore, improving the accuracy of shale gas well drillability predictions is a critical challenge. Rock drillability is a key parameter for optimizing drilling design and has established quantitative industry evaluation standards. However, most research has focused on vertical reservoir drillability, with limited studies on horizontal well reservoir drillability. Currently, rock drillability prediction methods mainly include laboratory micro-drillability experiments and log-based prediction approaches. He et al. (1998) conducted micro-drillability experiments on rock samples with different bedding angles and summarized the relationship between bedding inclination and drillability [1]. Chen et al. (2017) conducted extensive micro-drillability experiments, analyzing the effects of weight-on-bit and rotational speed on drillability ratings [2]. He proposed a new method for determining and classifying rock drillability using PDC micro-drill bits. However, these experiments were primarily conducted under ambient temperature and pressure conditions, which differ significantly from actual drilling environments. Yang (2014) developed a rock drillability testing apparatus that simulates high-temperature and high-pressure conditions [3]. His findings revealed fundamental differences in rock fragmentation behavior under such conditions compared to ambient conditions. Wei et al. (2016) Shandong et al. combined laboratory drillability testing with HyperMesh finite element simulations to investigate the impact of differential pressure variations on drillability [4]. The log-based prediction method has also made some progress. Gstalder et al. (1966), Mason et al. (1984), and Liu et al. (1995) suggested that laboratory acoustic data and logging data can be used to predict rock drillability [5–7]. Zou et al. (1996) analyzed the relationship between micro-bit drillability and acoustic transit time [8]. They refined the predictive model based on field data, improving its accuracy. Subsequently, Liang et al. (2006), Yang et al. (2010), and Geng et al. (2014) further integrated parameters such as rock density, bottom-hole confining pressure, and acoustic properties to enhance the accuracy of rock drillability prediction [9–11]. However, most researchers have relied on a single predictive method, overlooking the coupled effects of multiple factors. To this end, the innovations of this study lie in: (1) integrating multiple factors such as mineral composition, confining pressure, and bedding angle, and quantifying their coupling effects on drillability and (2) for the first time, applying intelligent optimization algorithms to the drillability model of shale horizontal wells, screening the optimal scheme by comparing Particle Swarm Optimization (PSO), Arithmetic Optimization Algorithm—Genetic Algorithm (AOA-GA), and Enhanced Binary Particle Swarm Optimization (EBPSO), and improving the prediction accuracy to a practical level. For instance, an increase in confining pressure may alter the influence of the drilling angle on drillability, while changes in mineral composition could affect the acoustic transit time characteristics of the rock. Overlooking these synergistic effects may reduce the accuracy of predictive models, introducing certain limitations in research. To address this issue, this study integrates drillability grading experiments, mineral composition analysis, and acoustic transit-time testing to examine the effects of mineral composition, acoustic transit time, bottom-hole confining pressure, and formation drilling angle on the drillability of horizontal well reservoirs. Based on these findings, a nonlinear regression model incorporating multiple parameters is developed and validated using field data. To enhance prediction accuracy, three intelligent optimization algorithms—PSO,

AOA-GA, and EBPSO—are applied to optimize the model, followed by performance evaluation, which yields relatively inferior results. Through systematic comparison of the optimization effects of the three algorithms, it is clarified for the first time that the EBPSO algorithm exhibits optimal performance in predicting the drillability of shale horizontal wells, providing a basis for algorithm selection in similar studies. The optimized model is then used to predict the drillability of Well D4, with results closely matching actual measurements, verifying its effectiveness. This study aims to enhance the prediction accuracy of shale gas well drillability, providing more reliable technical support for the efficient development of shale oil and gas reservoirs.

2. Laboratory Experiments

2.1. Experimental Methods and Equipment

Existing drillability grade values are either measured under atmospheric pressure or predicted using relevant mathematical models. Studies have shown that drillability grade values obtained under actual formation pressure conditions differ significantly from those measured under atmospheric pressure [3]. Similarly, the drillability predicted by mathematical models also deviates from the actual drillability of rocks under real conditions. Using a rock drillability testing apparatus with a micro-bit drilling method to evaluate rock samples under simulated bottom-hole conditions can effectively mitigate these issues [12]. The main parameters of the rock drillability tester are as follows: the experimental system supports a maximum confining pressure of 100 MPa, a pore pressure of 100 MPa, and a wellbore pressure of 100 MPa, with each pressure being independently controlled without interference. To simulate the effects of drilling parameters and bottom-hole fluid pressure on shale drillability, the experimental setup employs a static closed-loop servo control system. This system can replicate field conditions, including confining pressure, wellbore pressure, rock pore pressure, weight on bit (WOB), and rotational speed, as shown in Figure 1.

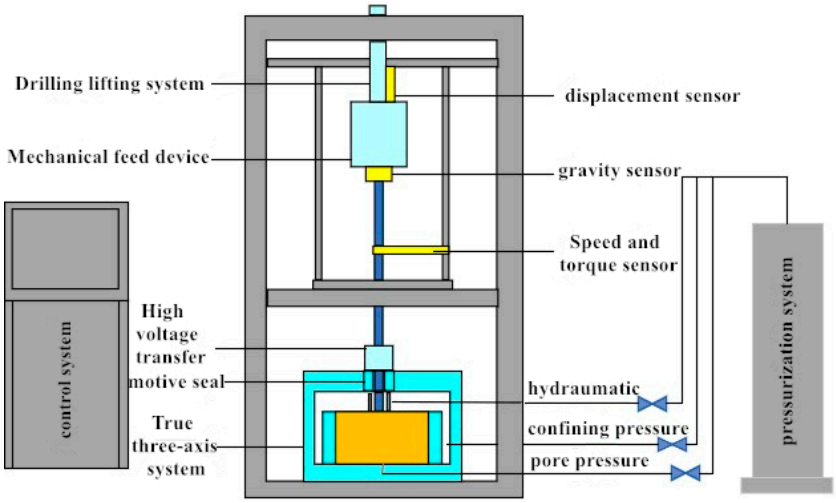

Figure 1. Diagram of drilling simulation experiment setup.

Using the rock drillability tester, a five-point drilling method was applied to the rock sample surface. A total of 21 experiments were conducted, and the collected data were processed to determine the drillability grade values, as shown in Figure 2.

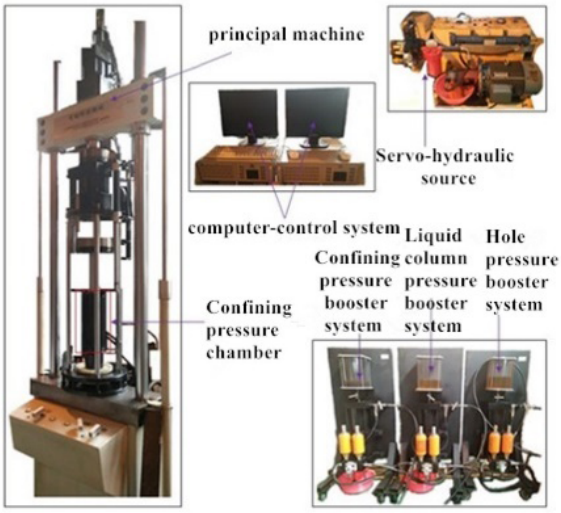

Figure 2. Drillability Tester.

To investigate the effects of WOB and rotational speed on rock-breaking efficiency, the following procedures were designed, considering the limitations of the equipment and rock samples: ① The WOB was set within a range of 0.25 kN to 1.25 kN. ② The rotational speed was set between 30 r/min and 150 r/min. ③ To quantify and characterize the rock-breaking efficiency of the PDC micro-bit under different drilling parameters, the efficiency was expressed in terms of the time required to drill a depth of 0.5 to 3.5 mm. ④ To examine the influence of bottom-hole pressure on shale drillability, micro-drilling experiments were designed with simulated bottom-hole pressures ranging from 10 MPa to 50 MPa.

2.2. Rock Sample Preparation

The experimental core samples were obtained from the Devonian shale reservoir in North America. This formation exhibits distinct bedding features. To ensure the integrity of the shale samples, specimens measuring 50 mm × 50 mm × 80 mm were collected in different orientations. To refine the rock samples, damaged surfaces were removed, and cylindrical samples (50 mm in diameter, 80 mm in length) were drilled at different angles (0°, 15°, 30°, 45°, 60°, 75°, 90°), as shown in Figure 3.

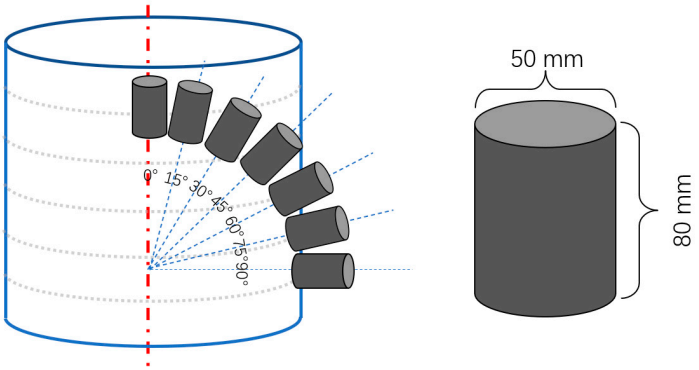

Figure 3. Schematic diagram of drilling parties and core samples.

2.3. Mineral Content Analysis of Shale Samples

To achieve a more accurate determination of the mineral content in the tested shale rock samples, X-ray diffraction XRD whole-rock analysis was employed to measure the mineral content of each rock sample, as shown in Table 1.

Table 1. Example of shale rock sample test results.

Number	Drooping Depth (m)	Sandpaper Content (%)	Clay Content (%)	Calcium Content (%)	Pressurization (MPa)	Sound Wave Time Lag (μs/m)	Stratigraphic Encounter Angle (°)	Drillability Rating
1	3172.98	31.3	22	30	29.11	243.32	−0.61	5.48
2	3186.98	37.5	41	15	29.12	185.17	−0.62	5.87
3	3195.85	38.4	39	13	29.16	250.23	0.52	5.99
4	3200.46	48.2	38	12	29.19	287.73	−0.32	6.11
5	3201.3	48.4	37	12	29.2	268.24	−0.31	6.15
6	3202.19	49	36	10	29.21	260.02	−0.34	6.19
7	3204.21	53	33	10	29.23	253.52	0.23	6.21
8	3204.85	53.1	33	10	29.25	222.15	0.24	6.25
9	3206.91	54.8	32	10	29.31	271.29	−0.32	6.37
10	3211.7	54.9	32	8	29.3	249.09	0.39	6.40
11	3213.33	55.2	32	8	29.33	256.04	0.45	6.46
12	3214.96	55.6	30	7	29.32	220.91	−0.42	6.49
13	3217.1	55.9	29	7	29.35	226.43	0.52	6.51
14	3221.0	55.9	26	7	29.39	290.48	0.63	6.54
15	3224.5	56.7	24	7	29.63	252.33	0.71	6.61
16	3230.0	57.8	24	7	29.47	179.69	−0.84	7.03
17	3231.0	63.1	20	7	29.32	253.51	0.88	7.08
18	3232.0	64.7	20	7	29.44	254.82	1.00	7.14
19	3232.7	66.1	19	6	29.52	200.94	−0.65	7.24
20	3232.5	66.1	19	6	29.61	250.32	1.11	7.92
21	3232.5	68	14	4	29.92	252.11	1.25	8.17

3. Analysis of Factors Affecting the Drillability of Horizontal Well Shale Reservoirs

3.1. Effect of Confining Pressure

The drillability grade values of shale under simulated confining pressures of 0 MPa, 10 MPa, 20 MPa, 30 MPa, 40 MPa, and 50 MPa were tested (Figure 4 shows the core before drilling, and Figure 5 shows the core after drilling). The results indicate that confining pressure has a significant impact on drillability grade values, as shown in Table 2. As the simulated confining pressure increased to 50 MPa, the drillability grade value increased by approximately 2 to 3 levels, as shown in Figure 6a. These test data provide crucial experimental support for developing a rock drillability prediction model.

Figure 4. Experimental core before drilling.

Table 2. Shale drillability test results under different peripheral pressures in Block D1 wells.

Case	Peripheral Pressure (MPa)					
	0	10	20	30	40	50
1	3.11	3.45	3.86	4.31	4.89	5.11
2	3.14	3.51	3.89	4.42	4.91	5.21
3	3.21	3.60	4.01	4.48	5.04	5.31
4	3.35	3.80	4.03	4.53	5.21	5.42
Average value	3.20	3.59	3.95	4.44	5.01	5.26

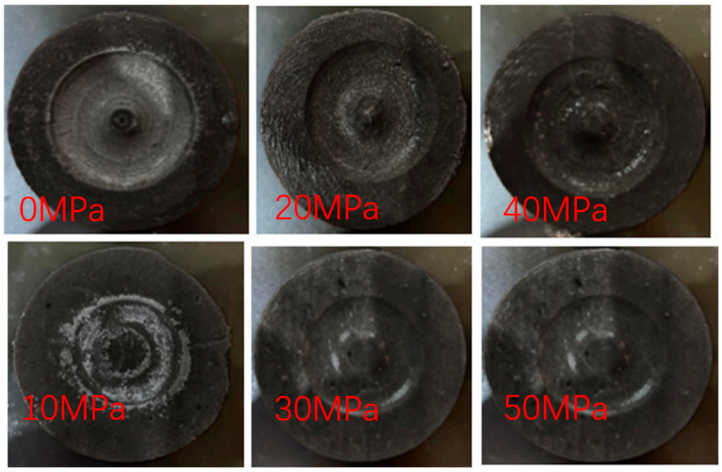

Figure 5. Experimental core after drilling.

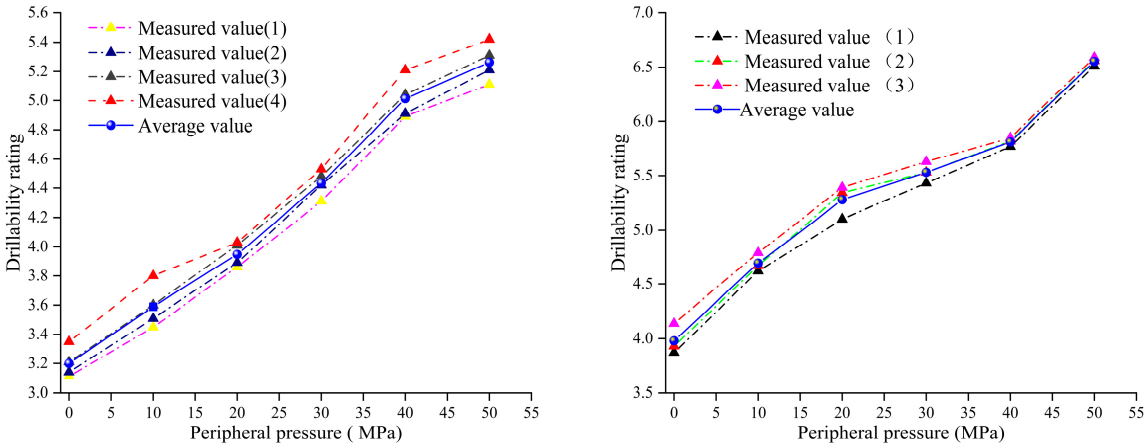

(**a**) Block X Well D1 Shale (**b**) Longmaxi Formation shale

Figure 6. Influence law of circumferential pressure on rock drillability.

Additionally, the drillability grade values of the Longmaxi Formation shale under different confining pressures were tested, further verifying the correlation between confining pressure and drillability grade values. According to the experimental results (Table 3 and Figure 6b), the drillability grade values increased correspondingly with increasing confining pressure.

Table 3. Shale drillability test results under different enclosing pressures in Sichuan Longmaxi Shale.

Case	Peripheral Pressure (MPa)					
	0	**10**	**20**	**30**	**40**	**50**
1	3.87	4.62	5.10	5.43	5.77	6.51
2	3.93	4.67	5.34	5.53	5.82	6.56
3	4.14	4.79	5.39	5.63	5.85	6.59
Average value	3.98	4.69	5.28	5.53	5.81	6.56

To evaluate the effect of confining pressure on drillability grade values, the drillability grade values obtained under different confining pressures were used as reference standards. The difference between the measured values under confining pressure and the standard values was used to quantify the impact of confining pressure on rock drillability, as shown in Table 4. The correlation between confining pressure and rock drillability is illustrated in Figure 7.

Table 4. Extent to which envelope pressure affects drillability.

Case	Peripheral Pressure (MPa)	Impact of Envelope Pressure on Drillability
1	0	0
2	10	3.67
3	20	3.90
4	30	4.45
5	40	4.62
6	50	5.41

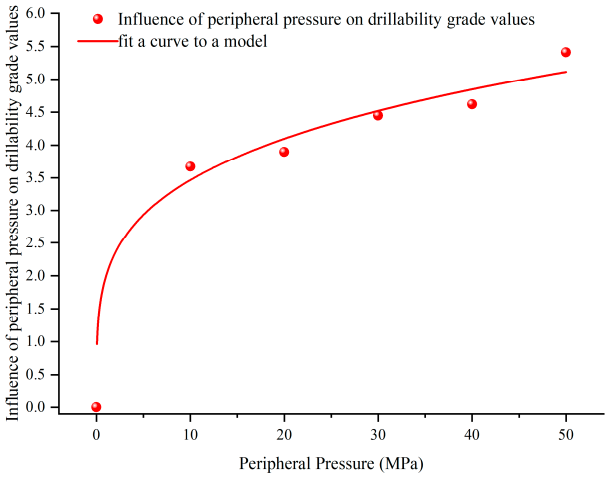

Figure 7. Correlation between envelope pressure and rock drillability.

A regression analysis was performed using the data from Table 4, and the resulting predictive model for the influence of confining pressure on rock drillability is given in Equation (1).

$$k_d = Ac_p^n \quad (1)$$

where A = 1.46, n = 0.28, and c_p represents the circumferential pressure in MPa.

The original data fitting performed well, with minimal residuals. The overall distribution follows the aforementioned exponential model, with a correlation coefficient of 0.65, indicating a moderate fitting accuracy.

3.2. Influence of Bedding Angle

Taking Well D1 as the research subject, this study conducted drilling tests at different bedding angles (0°, 15°, 30°, 45°, 60°, 75°, and 90°) to investigate their influence on drillability. Experimental results indicate that for shale with distinct bedding features, the worst micro-drilling performance and lowest drillability occur when the drill bit is perpendicular to the bedding plane (bedding angle = 0°). Conversely, the best micro-drilling performance and highest drillability occur when the drill bit is parallel to the bedding plane (bedding angle = 90°). At a bedding angle of 45°, micro-drilling performance surpasses that observed at 15° and 30°. The micro-drilling time records for shale drillability tests at different bedding angles are shown in Figure 8.

According to the SY/T 5426-2016, the drillability grade value is calculated using Equation (2) [13].

$$k_d = log_2^t + G_i \quad (2)$$

In this equation: k_d represents the drillability grade value; t denotes the average drilling time (s); G_i is the equivalent conversion grade value; and i represents the weight-on-bit grade (Level 1: G_1 = 0, Level 2: G_2 = 1, Level 3: G_3 = 3).

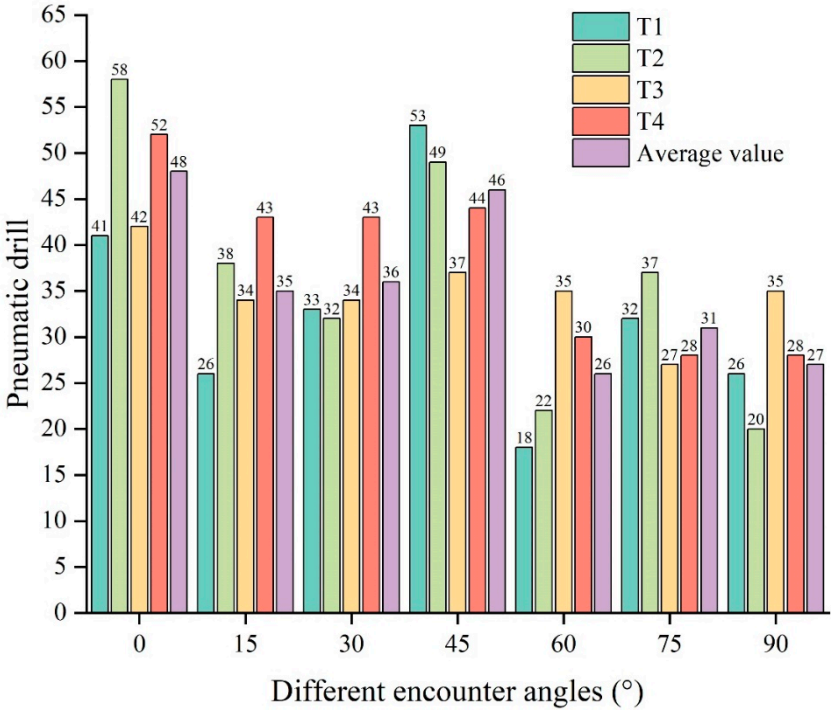

Figure 8. Microdrilling time logs of shale drillability experiments with different drilling angles.

In the triaxial drillability experiments, the influence of bedding angle on drillability was also tested under different confining pressures. As shown in Table 4, at low confining pressures (0–20 MPa), bedding angle significantly impacts shale drillability, with an average variation of 1.46. However, as the confining pressure increases (30–50 MPa), the impact of bedding angle gradually weakens. The relationship between bedding angle and drillability grade under different confining pressures is illustrated in Figure 9.

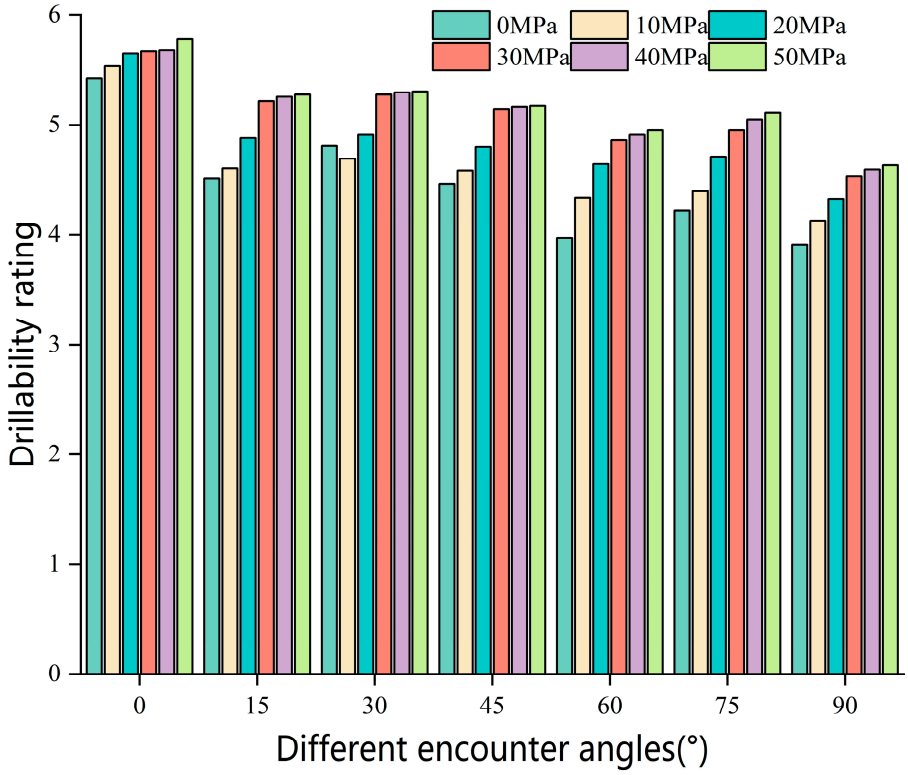

Figure 9. Influence of drilling encounter angle on drillability under peripressure conditions.

At a confining pressure of 30 MPa, the influence of bedding angle on drillability is significant. A nonlinear fitting was applied to derive the relationship between drillability grade and bedding angle, achieving a prediction accuracy of 0.73.

$$k_d = 0.73\cos(8\alpha) - 0.73 \quad (3)$$

where α represents the bedding angle.

3.3. Influence of Mineral Composition

Shale cuttings from the Devonian oil field block in North America, based on well-logging data, were analyzed for a comprehensive mineral composition assessment, as shown in Figures 10 and 11.

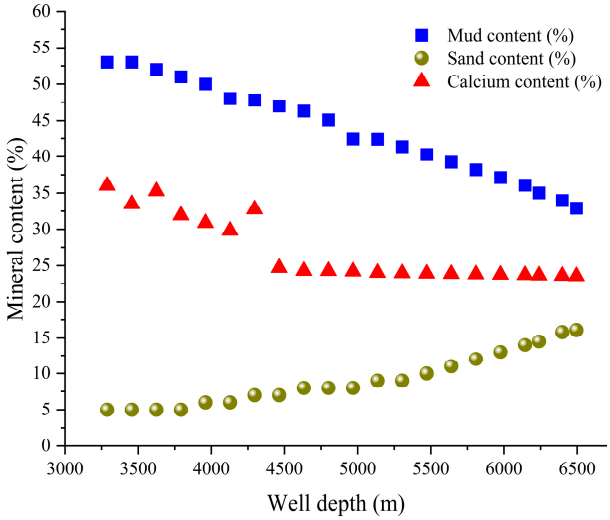

Figure 10. Plot of drillability grade values composition versus well depth.

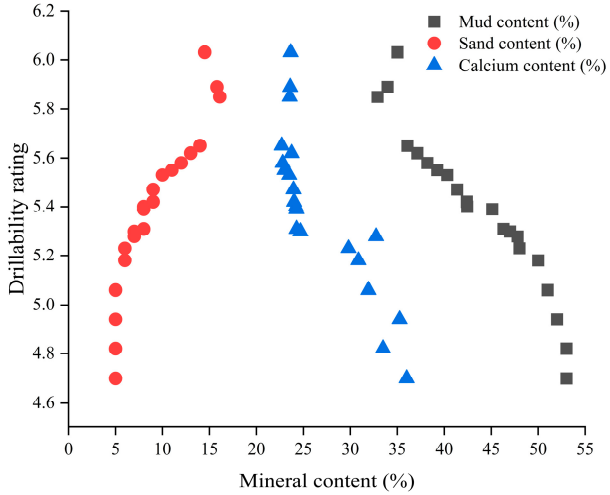

Figure 11. Plot of rock mineral content versus mineral composition.

Experimental results indicate that the primary mineral components of shale in this block include quartz, feldspar, calcite, plagioclase, and clay minerals. The analysis further reveals common characteristics: clay and plagioclase content decrease with depth, whereas quartz content increases. To reduce the modeling parameters for the drillability grade equation and decrease computational complexity, mineral components were categorized as sandy, argillaceous, and calcareous. As shown in Figures 10 and 11, argillaceous content decreases with depth, leading to a decrease in drillability grade. Sandy content increases

with depth, correlating with an increase in drillability grade. Calcareous content decreases between depths of 3100 m and 4500 m but stabilizes beyond 4500 m, showing minimal variation. The drillability grade stabilizes when calcareous content is approximately 8–10%.

Based on XRD experiments, scatter plots were generated with sandy content, argillaceous content, and calcareous content as the independent variables and shale drillability grade as the dependent variable. Goodness-of-fit selection determined that exponential and power functions were optimal for modeling drillability grade, with fitting accuracies of 0.67, 0.62, and 0.64, respectively. However, the fitting results were not highly ideal. The fitted equations are shown in Equations (4)–(6).

$$k_d = 4.03e^{0.0091}s_c \quad (4)$$

$$k_d = 17.34a_c - 0.29 \quad (5)$$

$$k_d = 10.98c_c - 0.24 \quad (6)$$

where k_d represents the rock drillability grade value (dimensionless); s_c denotes the sand content; a_c represents the clay content; and c_c refers to the carbonate content.

The correlation between shale drillability grade values and mineral content is shown in Figure 12.

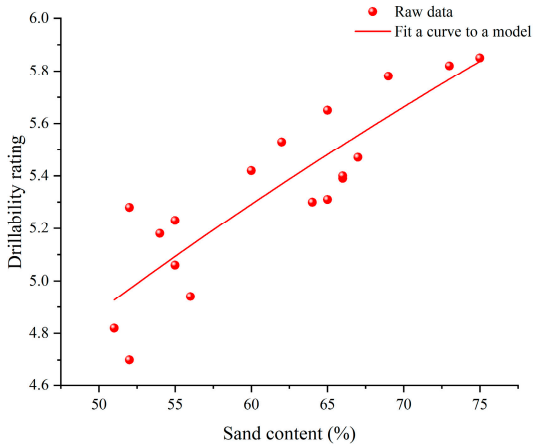

(**a**) Relationship between Sand Content and Drillability Rating

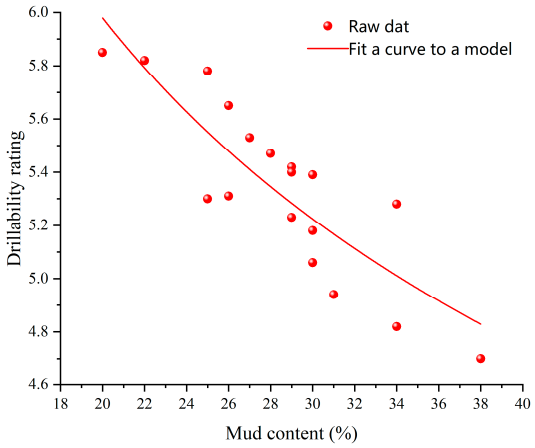

(**b**) Relationship between Mud Content and Drillability Rating

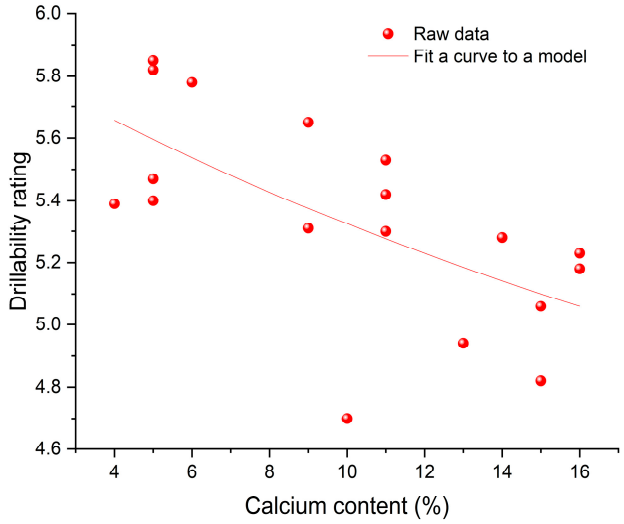

(**c**) Relationship between Calcium Content and Drillability Rating

Figure 12. Correlation between shale drillability grade value and mineral content.

As shown in Figure 12, clay content has a significant impact on the drillability grade value, whereas sand and carbonate content have relatively minor effects. Therefore, clay content can be considered the primary evaluation factor, while sand and carbonate content can serve as secondary factors.

3.4. Influence of Acoustic Transit Time

Experimental data indicate a strong correlation between acoustic transit time and drillability grade value, with a clear functional relationship. Specifically, the drillability grade value decreases as acoustic transit time increases. The smaller the acoustic transit time, the higher the drillability grade value, indicating greater rock hardness and increased difficulty in breaking.

A scatter plot was generated with the drillability grade value as the vertical axis and the compressional wave transit time as the horizontal axis. Based on the observed trend in the scatter plot, a power function was selected to fit the relationship between drillability and acoustic transit time, achieving a fitting accuracy of 0.78, as shown in Figure 13.

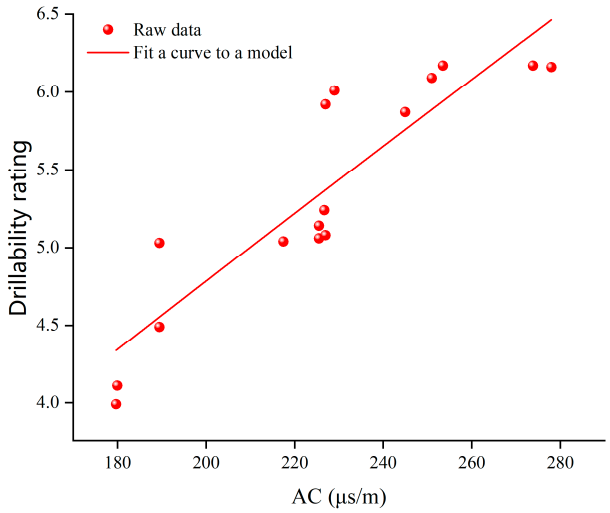

Figure 13. Drillability grade value vs. acoustic time difference curve.

As illustrated in Figure 13, acoustic transit time has a significant impact on the drillability grade value and serves as a critical influencing factor.

The regression fitting yielded a predictive model for the relationship between drillability grade value and compressional wave transit time:

$$k_d = 250.18AC^{-0.663} \tag{7}$$

where k_d represents the rock drillability grade value (dimensionless), and AC denotes the acoustic transit time (μs/m).

4. Construction of the Drillability Extremum Prediction Model

Given the heterogeneity of formations and the limitations of logging data, relying on a single-factor fitting approach is insufficient to comprehensively reflect rock drillability. This model breaks through the limitations of traditional single-factor fitting, and for the first time incorporates the coupling effects of mineral composition, acoustic transit time, confining pressure, and bedding angle into a unified framework, achieving a comprehensive characterization of drillability. Therefore, a nonlinear drillability prediction model was developed based on the fitting formulas established in Equations (1) and (3)–(7).

$$k_d = kAC^{a}e^{(bs_c+c\alpha)}a_c^d c_c^f ln(c_p) \tag{8}$$

where a, b, c, d, f, and k are coefficients.

By integrating the drillability grade test results of ten different types of shale, including calcareous shale, ferruginous shale, siliceous shale, carbonaceous shale, and black shale, along with the mineral composition and content from Table 1, bottomhole confining pressure, and formation inclination angle, regression analysis was conducted to determine the coefficients a, b, c, d, f, and k. The resulting multifactor shale drillability grade prediction model is as follows:

$$k_d = 0.922 \times 10^{-7} AC^{0.971} e^{(0.251S_c + 0.812\alpha)} a_c^{3.124} c_c^{0.193} ln(c_p) \quad (9)$$

(1) Establishment of the Prediction Model

To evaluate the accuracy of the established model, regression analysis was conducted based on the measured rock drillability values using statistical methods. The selection criteria for the regression equation included a higher correlation coefficient and larger test values, indicating stronger model correlation.

Given a confidence level of α = 0.01, the correlation coefficient test table and F(1,8) distribution table yield $R_{0.01,8}$ = 0.75 and a critical value of λ = 11.26. Clearly, when using a comprehensive multiparameter approach to predict rock drillability, $R > R_{0.01,8}$ and $F > \lambda$, indicating a significant test effect at a high confidence level. The coefficient of determination R^2 is 0.77, and the F-test value is 49.59, confirming that Equation (9) is a feasible predictive model for shale drillability in horizontal reservoir sections.

(2) Model Validation

For the drilled reservoir sections, the lithology of each sublayer, bottomhole pressure, and formation inclination angle were obtained. Based on the established nonlinear multiparameter rock drillability prediction model, the corresponding drillability grade values were computed. A comparative analysis was conducted using the drillability grade values measured in micro-drilling experiments for wells D2 and D3, as shown in Figure 14.

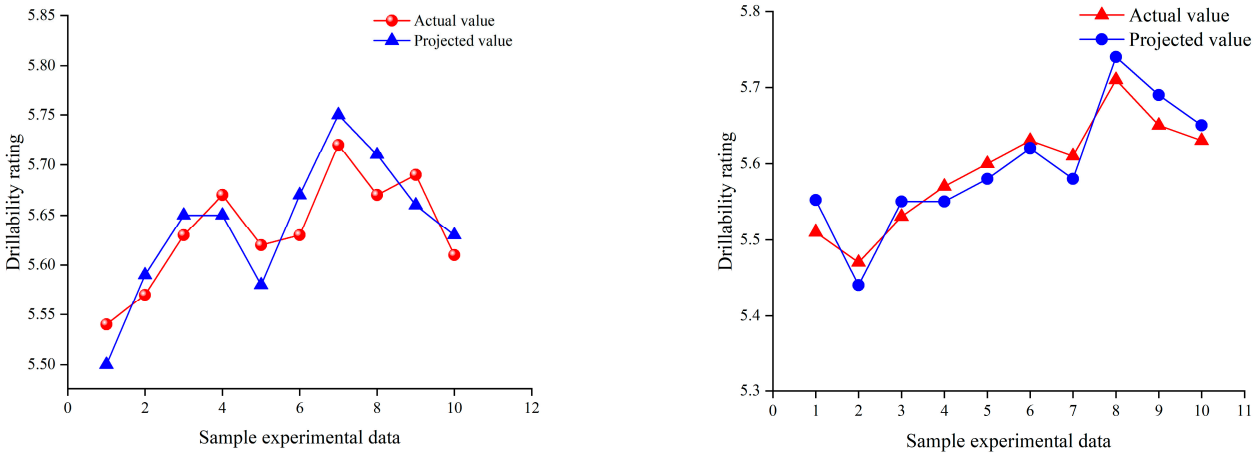

(**a**) Experimental data from Well D2 (**b**) Experimental data from Well D3

Figure 14. Sample plots of experimental data from wells D2 and D3.

To validate the predictive accuracy of the model, the root mean square error (*RMSE*), mean squared error (*MSE*), and mean absolute error (*MAE*) were used to evaluate wells D2 and D3. The formulas are as follows:

Root Mean Square Error (*RMSE*):

$$RMSE = \sqrt{MSE} = \sqrt{\frac{SSE}{n}} = \sqrt{\frac{1}{n}\sum_{i=1}^{m} w_i(y_i - \hat{y}_i)^2} \times 100\% \quad (10)$$

Mean Squared Error (*MSE*):

$$MSE = \frac{SSE}{n} = \frac{1}{n}\sum_{i=1}^{m} w_i(y_i - \hat{y}_i)^2 \times 100\% \quad (11)$$

Mean Absolute Error (*MAE*):

$$MAE = \frac{1}{n}\sum_{i=1}^{n} |\hat{y}_i - y_i| \times 100\% \quad (12)$$

The specific error analysis results are presented in Table 5.

Table 5. Comparison of validation well error analysis.

Verification Well	MAE	MSE	RMSE	R^2
Well D2	0.10	0.08	0.22	0.77
Well D3	0.06	0.07	0.19	0.76

The nonlinear multivariate regression prediction model for shale drillability grade values was validated using wells D1 and D2. As shown in Table 4, the R^2 values for wells D2 and D3 were 0.77 and 0.76, respectively, indicating moderate predictive performance. Therefore, further optimization of the nonlinear multivariate regression model is required to enhance prediction accuracy.

5. Model Improvement Based on Intelligent Optimization Algorithms

The predictive regression equation for horizontal reservoir drillability grade values, derived from the above methods, exhibits limitations due to its singularity, preventing optimal prediction accuracy. Therefore, machine learning optimization algorithms are introduced to enhance the predictive precision of the equation. The workflow of the machine learning optimization algorithm is shown in Figure 15 [14–16].

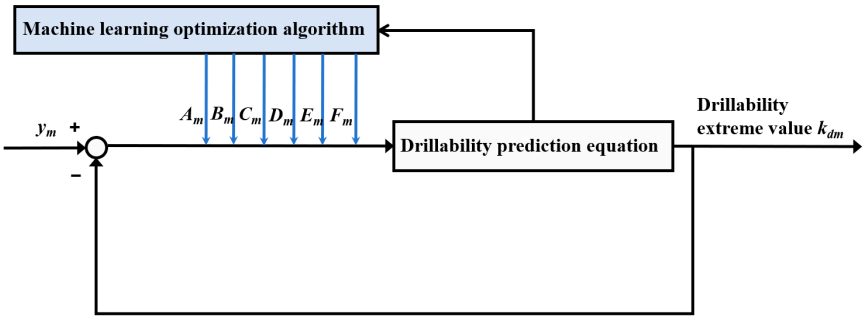

Figure 15. Process of optimizing prediction model parameters using machine learning algorithm.

5.1. Improvement of Model Equations Using Intelligent Optimization Algorithms

Mineral content testing indicates that the mineral composition and lithology variations within the reservoir section are minimal. This study selects the reservoir section of well D1 as an example to optimize the drillability grade value prediction equation. The workflow diagram is shown in Figure 16.

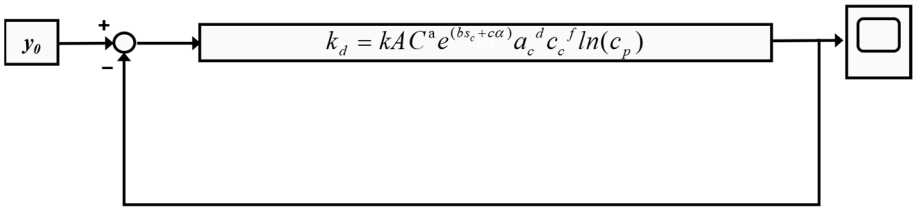

Figure 16. Prediction Model Calculation Block Diagram.

5.1.1. Optimization of the Predictive Equation Using the PSO Algorithm

The parameter settings are as follows: particle swarm size = 100, maximum number of iterations = 120. The iterative algorithm curve obtained is shown in Figure 17.

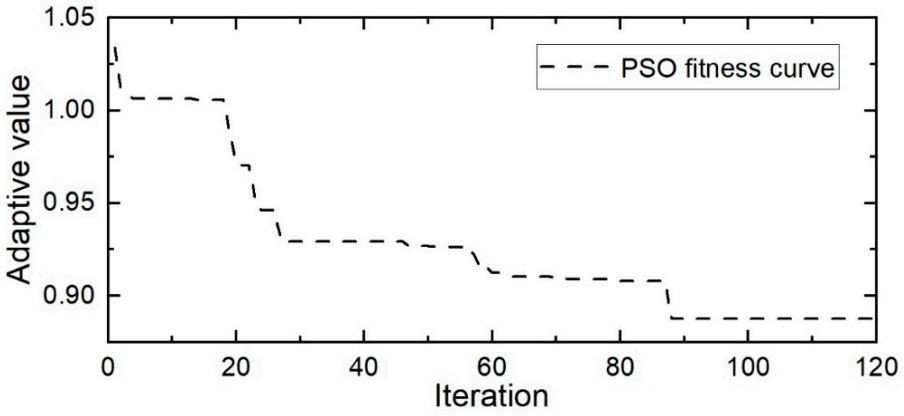

Figure 17. PSO fitness curve.

In this design, the integral of time-weighted absolute error (ITAE) is set as the objective function. The resulting algorithm curve is shown in Figure 18. As seen in Figure 18, the fitness value reaches its minimum at 23 iterations. Using MATLAB (R2024a) software, the PSO algorithm yields six adjustable coefficients for the horizontal well reservoir drillability grade prediction model: A4 = 0.33, B4 = 0.16, C4 = 0.22, D4 = 0.11, E4 = 0.27, and F4 = 0.34. At this point, the system performance reaches its optimum, achieving the best optimization results.

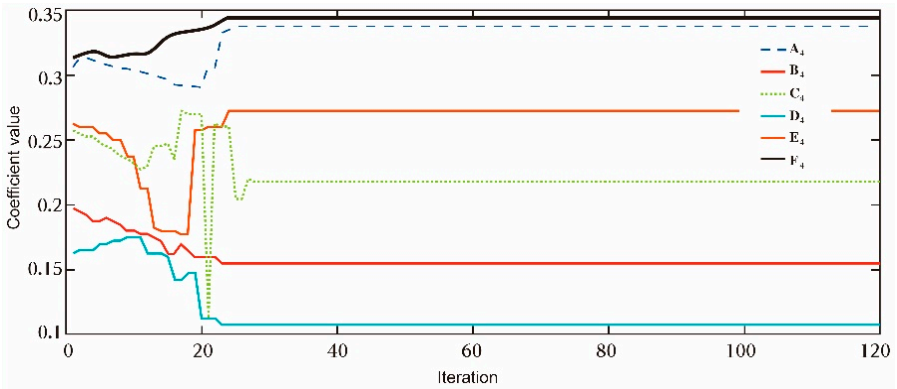

Figure 18. PSO prediction equation coefficient optimization value curve.

5.1.2. Optimization of the Predictive Equation Using the AOA-GA Algorithm

The parameter settings are as follows: population size = 100, maximum number of iterations = 120, crossover probability = 0.70, and mutation probability = 0.30. The iterative algorithm curve obtained is shown in Figure 19.

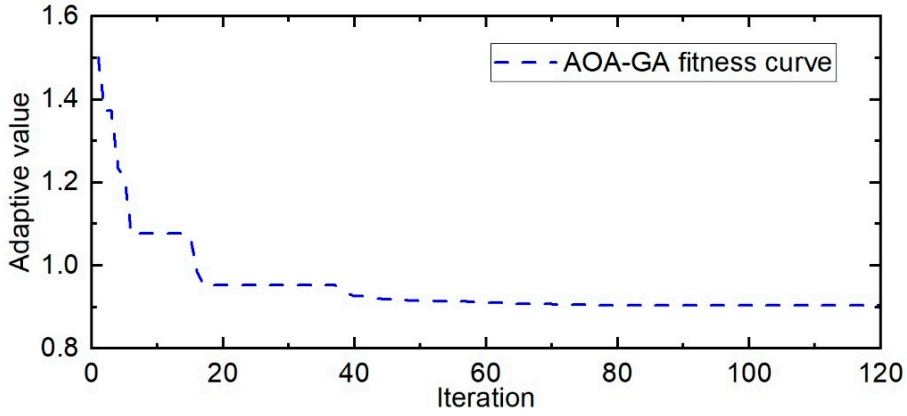

Figure 19. AOA-GA fitness curve.

In this design, the ITAE function is set as the objective function. The resulting algorithm curve is shown in Figure 20. As observed in Figure 20, the fitness value reaches its minimum at 25 iterations. Using MATLAB software, the AOA-GA optimization algorithm yields six adjustable coefficients for the horizontal well reservoir drillability grade prediction model: A4 = 0.25, B4 = 0.41, C4 = 0.21, D4 = 0.05, E4 = 0.02, and F4 = 0.23. At this point, the system performance reaches its optimum, achieving the best optimization results.

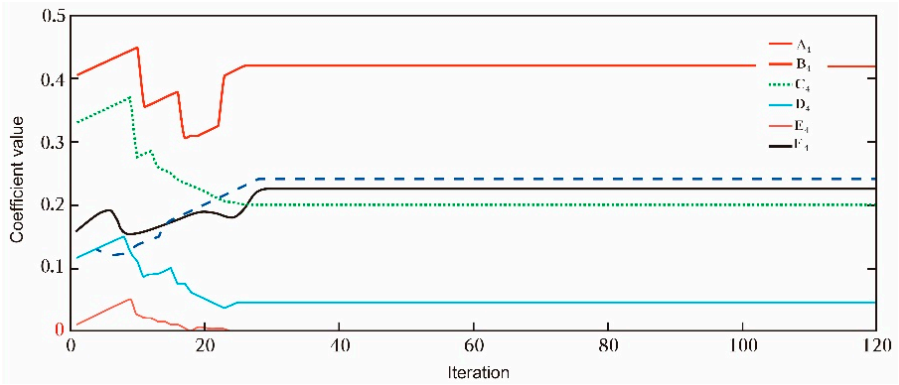

Figure 20. AOA-GA prediction equation coefficient optimization value curve.

5.1.3. Optimization of the Predictive Equation Using the EBPSO Algorithm

The parameter settings are as follows: using y4 as input, population size = 100, and maximum number of iterations = 120. The iterative algorithm curve obtained is shown in Figure 21.

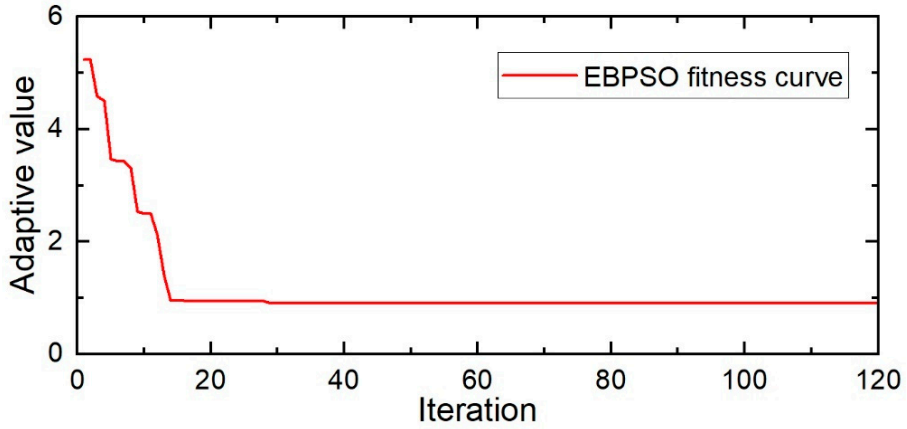

Figure 21. EBPSO fitness curve.

In this design, the ITAE function is set as the objective function. The resulting algorithm curve is shown in Figure 22. As seen in Figure 22, the fitness value reaches its minimum at 25 iterations. Using MATLAB software, the EBPSO algorithm yields six adjustable coefficients for the horizontal well reservoir drillability grade prediction model: A4 = 0.21, B4 = 0.42, C4 = 0.67, D4 = 0.05, E4 = 0.02, and F4 = 0.60. At this point, the system performance reaches its optimum, achieving the best optimization results.

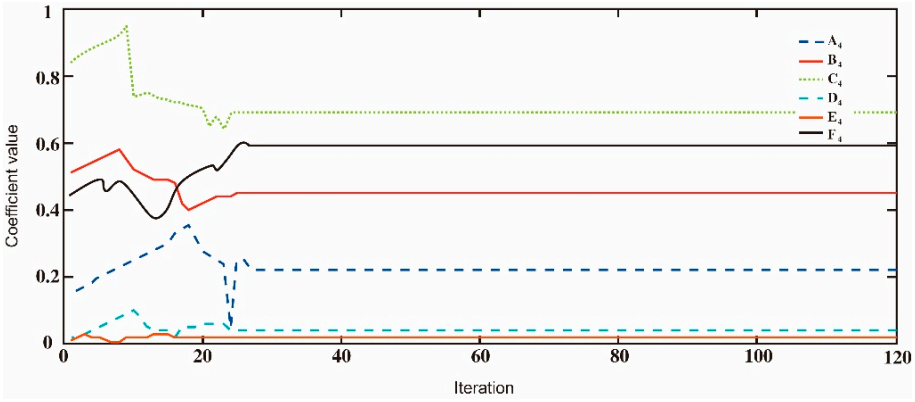

Figure 22. EBPSO prediction equation coefficient optimization value curve.

5.2. Performance Evaluation of the Intelligent Optimization Algorithm Model

Taking the Peak4 reservoir of well D1 as an example, the PSO algorithm, AOA-GA algorithm, and EBPSO algorithm were compared with the optimization results, as shown in Figures 23 and 24.

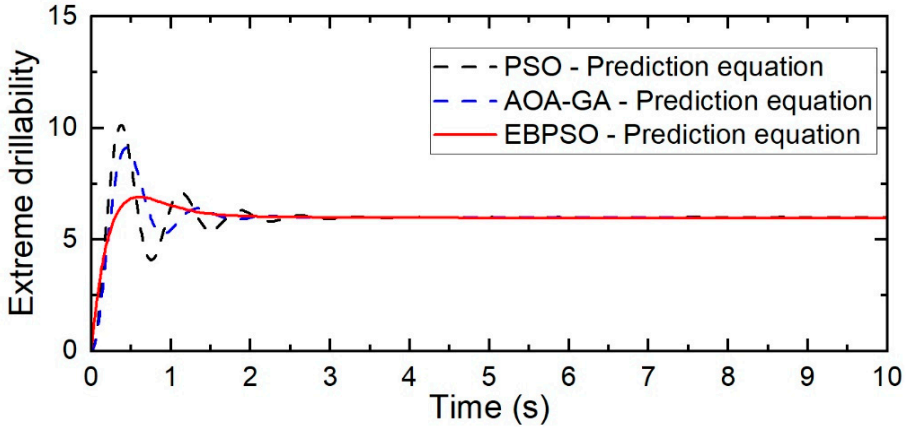

Figure 23. Comparison of Drillability Equations for Intelligent Optimization Algorithms.

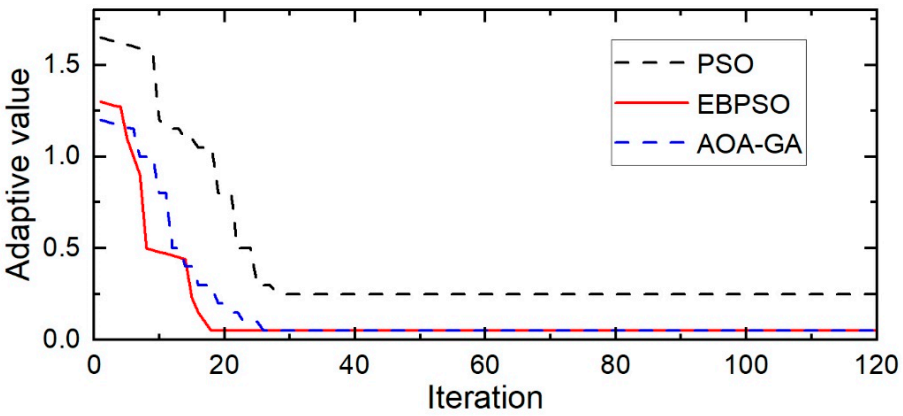

Figure 24. Comparison curve of fitness values of various algorithms.

As shown in Figures 23 and 24, the EBPSO algorithm achieves the minimum fitness value at the 18th iteration, the shortest time to reach the optimal prediction value, the lowest peak fluctuation, and the smallest variation range. The predicted drillability values obtained from the EBPSO algorithm are the closest to the experimental drillability values. Therefore, the EBPSO algorithm yields the best optimization results for the drillability prediction equation, followed by the AOA-GA algorithm, while the PSO algorithm performs relatively worse, as shown in Figure 25. The optimization results for other reservoir drillability values are presented in Table 6.

Table 6. Comparison of Prediction Results of Optimization Algorithms for D1 Well.

Formation	Optimization Algorithm	Peak Value (%)	Optimal Prediction Time (s)	Range of Fluctuation (%)	Optimized Drillability Level Value	Drillability Level Value Before Optimization	Actual Drillability Level Value	Root Mean Square Error
A	PSO	10.2	2.54	40.5	5.13	5.15	5.06	0.07
	AOA-GA	8.6	2.27	36.6	5.10			0.04
	EBPSO	6.3	1.95	24.9	5.09			0.03
B	PSO	11.2	2.70	41.2	5.22	5.36	5.28	0.06
	AOA-GA	9.7	2.41	35.7	5.31			0.03
	EBPSO	7.1	2.07	23.1	5.26			0.02
C	PSO	10.8	2.57	42.1	5.27	5.23	5.39	0.12
	AOA-GA	8.7	2.31	35.5	5.31			0.10
	EBPSO	6.9	2.01	25.2	5.34			0.08
Peak1	PSO	11.1	2.65	42.4	5.21	5.31	5.27	0.06
	AOA-GA	8.9	2.49	36.3	5.24			0.03
	EBPSO	6.8	1.98	26.8	5.29			0.02
Peak1_carb	PSO	12.1	2.81	41.5	5.73	5.70	5.82	0.09
	AOA-GA	10.7	2.53	35.7	5.75			0.07
	EBPSO	7.9	2.24	26.3	5.76			0.06
Peak2	PSO	10.8	2.57	40.6	4.73	4.72	4.82	0.09
	AOA-GA	8.4	2.23	34.2	4.75			0.07
	EBPSO	6.2	1.91	24.8	4.78			0.04
Peak3	PSO	10.3	2.56	39.9	4.67	4.81	4.73	0.06
	AOA-GA	9.1	2.30	36.1	4.78			0.05
	EBPSO	6.7	2.01	23.7	4.76			0.03
Peak4	PSO	10.9	2.61	41.1	5.42	5.41	5.48	0.06
	AOA-GA	8.8	2.34	37.3	5.43			0.05
	EBPSO	6.4	2.03	24.4	5.52			0.04
Peak5	PSO	11.4	2.77	42.9	5.16	5.15	5.21	0.05
	AOA-GA	9.3	2.52	37.2	5.18			0.03
	EBPSO	7.1	2.17	25.8	5.22			0.01
Peak5_carb	PSO	12.6	2.86	43.3	5.87	5.93	5.82	0.05
	AOA-GA	11.1	2.62	35.7	5.78			0.04
	EBPSO	8.4	2.41	26.9	5.80			0.02
Peak6	PSO	11.5	2.81	40.5	5.32	5.33	5.27	0.05
	AOA-GA	9.6	2.57	35.8	5.30			0.03
	EBPSO	7.2	2.20	25.1	5.29			0.02
Peak7	PSO	10.4	2.61	41.3	4.79	4.77	4.83	0.04
	AOA-GA	9.1	2.39	34.7	4.86			0.03
	EBPSO	6.9	2.11	25.4	4.84			0.01

By comparing the drillability grade values obtained using the PSO, AOA-GA, and EBPSO algorithms with the unoptimized values, as shown in Table 6 and Figure 25, it is observed that the average peak values for the PSO, AOA-GA, and EBPSO algorithms are 11.1%, 9.6%, and 6.99%, respectively. The average optimal prediction times are 2.67 s, 2.63 s, and 2.09 s, while the average fluctuation ranges are 41.44%, 35.90%, and 25.20%, respectively. The average root mean square errors (RMSE) compared to actual values are 0.067, 0.045, and 0.029, respectively, whereas the RMSE before optimization was 0.09. This confirms that the optimized drillability grade values exhibit significantly higher predictive accuracy than the unoptimized values.

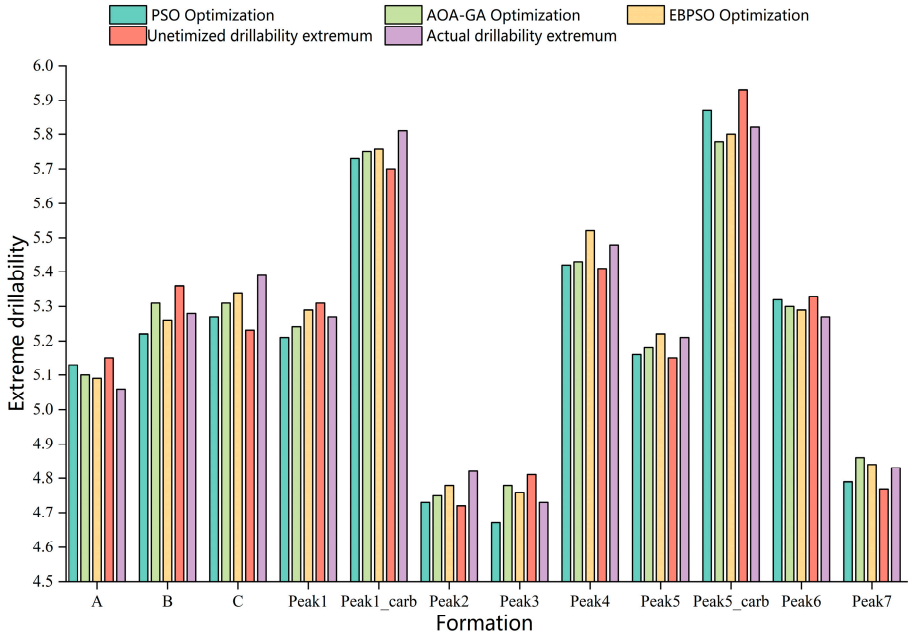

Figure 25. Comparison of drillability level values before and after optimization.

In summary, the predictive accuracy of drillability grade values is significantly improved after optimization. Among the algorithms, the improved binary particle swarm optimization (EBPSO) algorithm provides the best predictive performance, followed by the arithmetic optimization–genetic algorithm (AOA-GA), while the particle swarm optimization (PSO) algorithm performs the worst.

6. Case Study

The Duowone Block is located on the edge of the Western Canada Basin, a vast basin covering approximately 1688 km^2, spanning a large area between the United States and Canada. The basin's tectonic evolution occurred during the Devonian, Carboniferous, Late Permian, Jurassic to Early Cretaceous, and Middle to Late Jurassic–Tertiary periods. Among these, the Late Permian and Late Jurassic–Tertiary tectonic movements played a decisive role in shaping the basin's scale, stratigraphic development, and spatial distribution. The primary sedimentary formations consist of Paleozoic to Jurassic carbonates and mudstone, as well as Middle Jurassic to Paleocene clastic rocks. The study well is located in the western part of the Western Canada Basin, with the target shale situated in Devonian formations, characterized as deep-marine deposits. The lithology mainly comprises bitumen-rich dark black and black-gray siliceous and calcareous mudstone. The target shale has a thickness ranging from 20 to 35 m, with burial depths between 2500 and 3500 m [17]. The lithology of this formation exhibits characteristics such as high density, hardness, and strong anisotropy. To address these challenges, the nonlinear multiple regression drillability prediction model (Equation (8)) was utilized, along with model optimization, to validate the drillability values of well D4 in the shale formation.

A detailed analysis was conducted on the mineral composition, confining pressure, sonic travel time, and formation dip angle for each sublayer of well D4, as illustrated in Figures 26 and 27.

Due to the difficulty of obtaining core samples from the wellbore, it was not possible to verify the drillability values of each reservoir segment individually. To better estimate the reservoir drillability values, the relatively small variations in drillability values between sublayers were utilized. The wellbore trajectory of well D4 is shown in Figure 28.

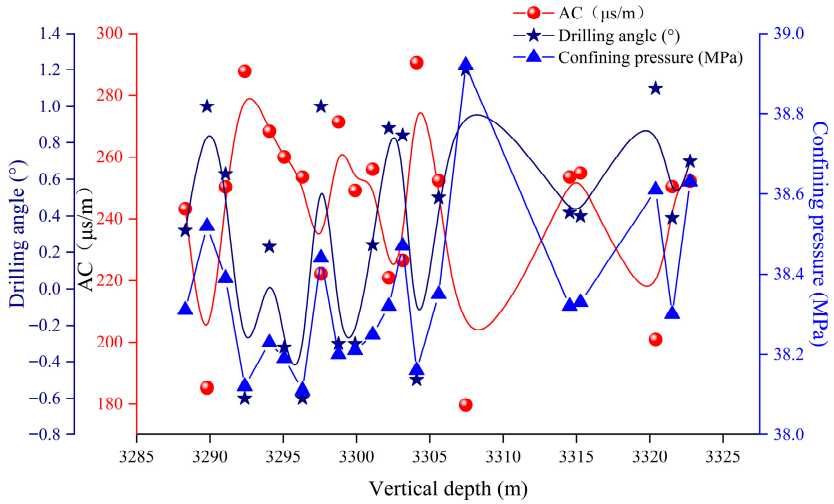

Figure 26. Variation in perimeter pressure, acoustic time difference, and stratigraphic encounter angle with plunge depth for well D4.

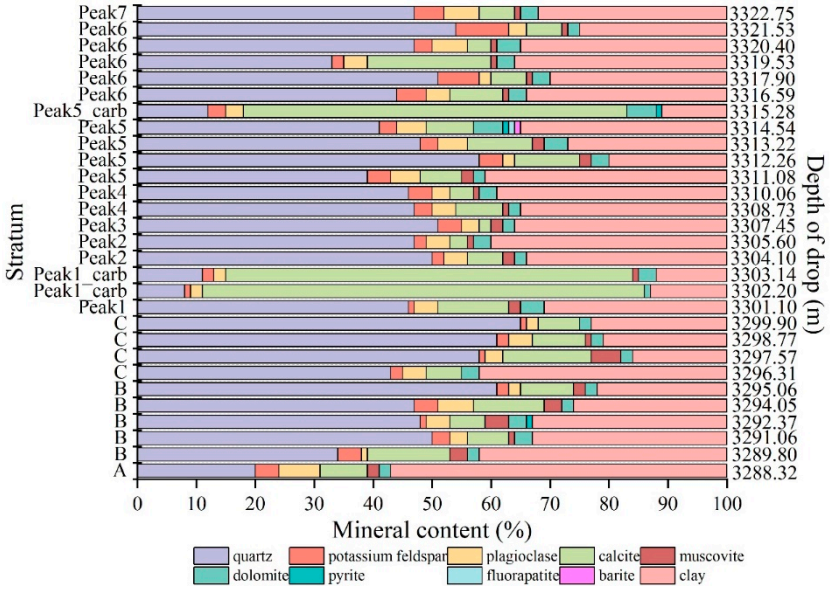

Figure 27. Distribution of mineralogical fractions in the Canadian Duvernay Shale reservoir at well D4.

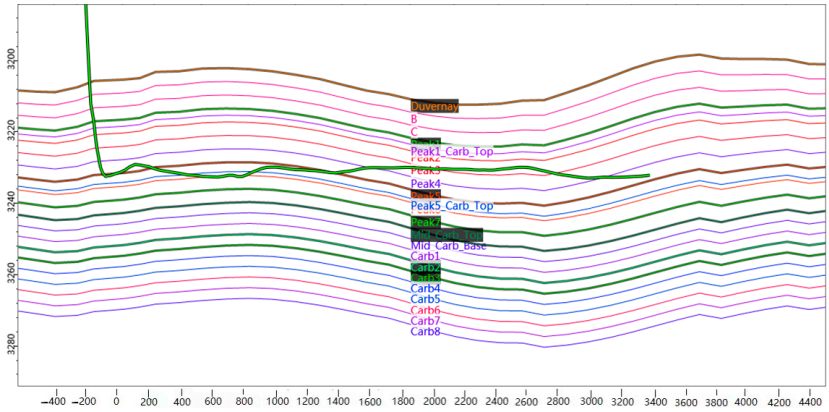

Figure 28. D4 well borehole trajectory.

In Figure 28, the "L" shaped green curve is the wellbore trajectory. The wellbore trajectory intersects multiple sublayers, including A, B, C, Peak1, Peak1_Carb_Top, Peak2,

Peak3, Peak4, Peak5, and Peak5_Carb_Top. Core samples were taken from six points at depths of 3923 m (Peak2), 4225 m (Peak5), 4824 m (Peak4), 5220 m (Peak5), 5810 m (Peak3), and 6013 m (Peak5) for experimental validation. The results are shown in Table 7.

Table 7. Experimental data table for experimental sites.

Case	Stratum	Well Depth (m)	Sand Content (%)	Mud Content (%)	Calcium Content (%)	AC (μs/m)	Well Bottoming Pressure (MPa)	Drilling Angle (°)	Predicting Drillability Grade Values	Actual Drillability Grade Value
A1	Peak2	3923	38	36	11	250.23	38.35	−0.32	5.351	5.345
A2	Peak5	4225	38	35	10	251.61	38.63	0.22	5.357	5.361
A3	Peak4	4824	43	31	8	250.62	38.71	0.35	5.566	5.560
A4	Peak5	5220	40	35	13	251.27	38.72	0.31	5.375	5.361
A5	Peak3	5810	30	41	16	251.12	38.91	−0.19	5.064	5.072
A6	Peak5	6013	37	39	14	251.36	38.54	0.31	5.363	5.349

A comparison of the predicted and actual drillability extreme values is presented in Figure 29.

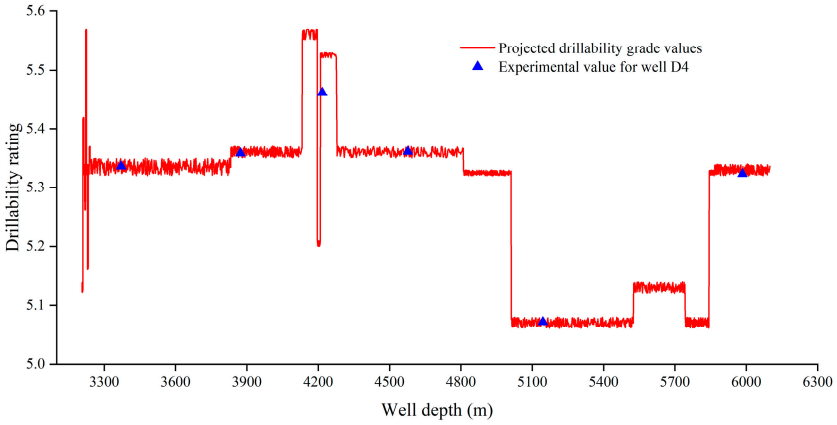

Figure 29. Presentation of the results of the validation well D4 with nonlinear multivariate regression of the drillability grade values.

The predicted values closely match the experimental values for five of the points. However, at the 4200 m experimental point, there is a significant deviation between the predicted and experimental values. This discrepancy may be attributed to lithological variations, faults, fractures, or folds in the geological structure, resulting in abrupt changes in local geological conditions. Overall, the results obtained from the reservoir drillability prediction model align well with the actual values, demonstrating that the model provides high prediction accuracy.

In summary, as shown in Figure 29, the drillability grade values are generally consistent with the results predicted by the nonlinear multivariate regression drillability model established in Equation (8). Therefore, Equation (8) can be confirmed as a valid predictive model for the drillability grade of shale reservoirs. This model enables the rapid construction of a drillability profile for horizontal shale reservoir wells and provides insights into their distribution patterns. Consequently, it offers a valuable reference for drill bit selection in new wells, serving as a practical guide for improving the mechanical drilling speed in shale formations.

7. Conclusions and Recommendations

(1) Through drillability grade experiments and mineral composition analysis, the effects of mineral composition, acoustic travel time, bottom-hole confining pressure, and formation encounter angle on drillability were investigated. The results show that

confining pressure has the most significant impact on drillability grade: when the confining pressure increases to 50 MPa, the drillability grade improves by 2–3 levels. In the range of 0–20 MPa, the encounter angle has a considerable influence on drillability; however, this effect weakens as the confining pressure increases to 30–50 MPa. Additionally, the drillability grade decreases with increasing acoustic travel time and stabilizes around 250 μs/m. These findings lay a foundation for the subsequent multi-parameter coupling analysis, distinguishing our study from single-factor-focused studies.

(2) A nonlinear regression predictive model was developed to describe the relationship between multiple parameters and the drillability of horizontal well reservoirs, validated using data from wells D1 and D2. By integrating mineral composition, acoustic travel time, confining pressure, and encounter angle into a unified framework, this model breaks through the limitations of traditional single-parameter prediction methods. The results indicate that the model effectively captures the trend of drillability variations, though its predictive accuracy requires further refinement—addressing a key gap in existing research that overlooks parameter coupling effects.

(3) To improve predictive accuracy, three intelligent optimization algorithms—particle swarm optimization (PSO), arithmetic optimization algorithm combined with genetic algorithm (AOA-GA), and enhanced binary particle swarm optimization (EBPSO)—were employed to optimize the model parameters and assess their performance. The results reveal that the EBPSO algorithm achieved the best optimization performance, followed by AOA-GA, while the PSO algorithm was comparatively less effective. A case study on well D4 validated the accuracy of the optimized model, demonstrating its ability to more accurately predict the drillability grade of shale reservoirs. This systematic comparison of intelligent algorithms, for the first time, confirms EBPSO's optimal applicability in shale horizontal well drillability prediction, providing a reliable basis for drilling parameter optimization and drill bit selection.

The core innovations of this study are: (1) establishing a multi-parameter coupled drillability prediction model that overcomes the limitations of single-parameter approaches by quantifying the synergistic effects of mineral composition, acoustic travel time, confining pressure, and encounter angle and (2) enhancing model accuracy through intelligent optimization algorithms, with EBPSO validated as the most effective, thus offering an innovative technical method for the efficient development of shale horizontal wells.

Author Contributions: Conceptualization, Y.Z. and Q.W.; methodology, W.W.; software, Q.W.; validation, H.Z., Y.Z. and K.S.; formal analysis, H.W.; investigation, M.L. (Mingzhong Li); resources, M.L. (Meng Li); data curation, W.W.; writing—original draft preparation, Y.Z. and Q.W.; writing—review and editing, M.L. (Meng Li); visualization, Y.Z. and W.S.; supervision, Y.Z.; project administration, M.L. (Meng Li); funding acquisition, K.S. and M.L. (Meng Li). All authors have read and agreed to the published version of the manuscript.

Funding: This work was supported by the National Natural Science Foundation of China, [51974052], the Natural Science Foundation Project of Chongqing [CSTB2022NSCQ-MSX1403], Chongqing University of Science and Technology Youth Science and Technology Top Talent Cultivation Program Project [ckbjrc 202106], Technology Innovation Center for Directional Drilling Engineering, Ministry of Natural Resources [KF202401].

Data Availability Statement: Some of the data involved in this study are confidential information due to restrictions imposed by relevant company regulations and cannot be publicly accessed at this time. If relevant researchers or institutions need to use confidential data in this study reasonably for academic research purposes, they can contact the author Qiang Wang (contact information:

wangqiangjjsc@126.com). On the premise of strictly complying with relevant confidentiality agreements and laws and regulations, obtain the corresponding data after review and approval.

Acknowledgments: The author sincerely thanks SINOPEC Research Institute of Petroleum Engineering Co., Ltd. for providing valuable administrative support throughout the entire research process, greatly promoting the smooth progress of the research. We also appreciate the professional technical assistance provided by Chongqing University of Science and Technology, especially in software usage, data processing and analysis, which has made significant contributions to the completion of this work. In addition, we would like to express our gratitude to Sinopec Huabei Oilfield Service Company for donating experimental samples, which are crucial for conducting the experiments described in this manuscript. In the process of writing this manuscript, no GenAI tools were used to generate text, data, graphics, research design, data collection, analysis, or data interpretation.

Conflicts of Interest: Authors Yanbin Zang, Hongning Zhang, Heng Wang were employed by the company SINOPEC Research Institute of Petroleum Engineering Co. Authors Wei Wang was employed by the company Sinopec North China oil & Gas Company. Authors Mingzhong Li, Wenyu Song were employed by the company Sinopec Huabei Oilfield Service Company. The remaining authors declare that the research was conducted in the absence of any commercial or financial relationships that could be construed as a potential conflict of interest. The funders had no role in the design of the study; in the collection, analyses, or interpretation of data; in the writing of the manuscript; or in the decision to publish the results.

Abbreviations

The following abbreviations are used in this manuscript:

XRD	X-ray diffraction
PSO	Particle Swarm Optimization
AOA-GA	Arithmetic Optimization Algorithm–Genetic Algorithm
EBPSO	Enhanced Binary Particle Swarm Optimization

References

1. He, S.; Xia, Y. Study on the influence of stratigraphic dip on the drillability of rocks. *Drill. Min. Technol.* **1998**, *1*, 11–15.
2. Chen, H. Research on Rock Drillability Determination and Grading Method of PDC Drill Bit. Master's Thesis, Southwest Petroleum University, Chengdu, China, 2017.
3. Yang, W. Experimental Research on Drillability of Rock at High Pressure and High Temperature. Master's Thesis, Southwest Petroleum University, Chengdu, China, 2014.
4. Wei, S.; Meng, Y.; Shi, X.; Tang, H. Experimental and simulation study of rock drillability under wellbore pressure conditions. *Sci. Technol. Eng.* **2016**, *16*, 271–274+285.
5. Gstalder, S.; Raynal, J. Measurement of some mechanical properties of rocks and their relationship to rock drillability. *J. Pet. Technol.* **1966**, *18*, 991–996. [CrossRef]
6. Mason, K.L. *Tricone Bit Selection Using Sonic Logs*; No. CONF-8409104; Amoco Production Co.: Terry County, TX, USA, 1984.
7. Liu, W.D. A new method for predicting rock drillability using sonic time difference. *Drill. Process* **1995**, *2*, 1–3.
8. Zou, D.-Y.; Chen, Y.-H. Study on the determination of rock drillability by using acoustic time difference data. *Oil Drill. Process* **1996**, 27–30+97. [CrossRef]
9. Liang, Q.M.; Zou, D.Y.; Zhang, H.W.; Li, X.Q. Experimental study on the comprehensive prediction of rock drillability using logging data. *Oil Drill. Technol.* **2006**, *1*, 17–19.
10. Yang, M.; Meng, Y.; Li, F.; Li, Y.; Wang, Y. Research on the Drillability of Bottom Rock under Different Drilling Methods. *Pet. Drill. Technol.* **2010**, *38*, 19–22.
11. Geng, Z.; Fan, H.; Chen, M.; Wang, J.; Ji, R.; Jing, N. Research and Application of Prediction Method for Regional Three dimensional Rock Drillability. *Pet. Drill. Technol.* **2014**, *42*, 80–84.
12. Lin, C.; Zhang, X.; Zhao, X. A review of indoor research methods for sedimentary petrology. *J. Paleogeography* **2021**, *23*, 223–244.
13. *SY/T 5426-2016*; Drilling Engineering for the Petroleum and Natural Gas—Rock Drillability Measurement and Its Grading. National Energy Administration: Beijing, China, 2016.
14. Zhang, J.; Ding, S.; Li, B. Improved Particle Swarm Optimization based Support Vector Machine Feature Selection and Parameter Joint Optimization Algorithm. *Comput. Appl.* **2016**, *36*, 1330–1335.

15. Gupta, S.; Gupta, S. Fitness and historical success information-assisted binary particle swarm optimization for feature selection. *Knowl.-Based Syst.* **2024**, *306*, 112699. [CrossRef]
16. Ma, L.; Dai, C.; Xue, X.; Peng, C. A Multi-Objective Particle Swarm Optimization Algorithm Based on Decomposition and Multi-Selection Strategy. *Comput. Mater. Contin.* **2025**, *82*, 997–1026. [CrossRef]
17. Huai, Y.; Qu, L.; Zhang, M.; Tan, Y.; Xia, C. Research on Logging Evaluation of Shale Gas Reservoirs in the Western Canada Basin, Canada. *China Min.* **2018**, *27*, 169–174.

Disclaimer/Publisher's Note: The statements, opinions and data contained in all publications are solely those of the individual author(s) and contributor(s) and not of MDPI and/or the editor(s). MDPI and/or the editor(s) disclaim responsibility for any injury to people or property resulting from any ideas, methods, instructions or products referred to in the content.